SAR Simulations and Experiments for Parallel Transmission

I. Graesslin[1], K. Falaggis[1], S. Biederer[1], D. Glaesel[1], P. Vernickel[1], P. Roeschmann[1], C. Leussler[1], A. Thran[1], Z. Zhai[2], M. Morich[2], and U. Katscher[1]

[1]Philips Research Europe, Hamburg, Germany, [2]Philips Medical Systems, Cleveland, Ohio, United States

Introduction

Parallel transmission [1-3] bears the potential of compensating B_1 field inhomogeneities induced by wave propagation effects for (ultra) high field whole body imaging. The RF power deposition and the associated local specific absorption rate (SAR) represent a specific attention point with respect to patient safety. Up to now SAR simulations and experiments have been analyzed only for a head-size homogeneous phantom using a four-channel parallel transmit system [4,5]. This paper presents simulations using a whole body human bio-mesh model and an eight-channel transmit/receive body coil [6]. SAR simulations were performed on a cuboid phantom, and validated by temperature measurements to asses safety and coil performance of an 8-channel transmit/receive body coil operating at 128MHz.

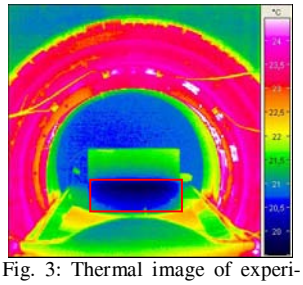

Fig. 3: Thermal image of experimental setup of phantom located in the MBC of the MRI system.

Methods

Simulations for objects located in a 3T multi-channel body coil (MBC) with eight ideally decoupled TEM transmit elements were carried out using the finite-difference time-domain (FDTD) method ("XFDTD", Remcom, Inc., USA). The MBC was simulated loaded with different phantoms using a 5mm grid and Perfectly Matched Layer boundaries (16 layers). As a bio-mesh, the model of the "Visible Human Male" [7] was used. The resulting field distributions were calculated by superposition of the single fields generated by the individual coil elements. The 2D spatially selective RF excitation pulses used for the examples were calculated iteratively in the spatial domain using a conjugate-gradient method [8]. Two local excitations were selected: a segmented region of the kidney (Fig. 1 top) as well as of the liver (Fig.1 bottom). Furthermore, other patterns including stochastic excitation patterns with varying numbers of excited pixels were evaluated using spiral k-space trajectories with a numerical field-of-excitations between 32×32 and 128×128 pixels. The Transmit SENSE pulses were calculated using reduction factors of up to eight. The SAR was calculated based on the computed E-fields derived from the FDTD simulations.

SAR verification experiments were carried out on an integrated 3T MRI prototype system [9] (based on Achieva, Philips, Netherlands) equipped with an eight-channel body coil. The latter was loaded with a homogeneous cuboid phantom (h=10cm, w=20cm, l=30cm) filled with a lipid-doped H20-NaCl-TX150 solution (σ=0.5S/m, ε_r=78). For the heating experiment, a continuous wave RF power of 50-200W was applied, for up to 45 minutes using up to eight transmit elements of the body coil simultaneously. The temperature measurements were carried out with a 4-channel fiber optic probe (Luxtron790, Santa Clara, CA) and an IR-camera (VarioTHERM, JENOPTIC, Jena, Germany).

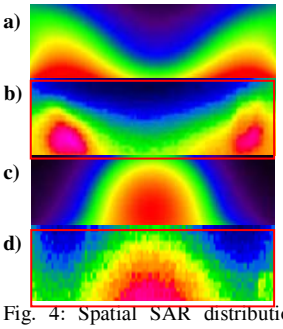

Fig. 4: Spatial SAR distribution simulation a) & c) and measured temperature b) & d) after heating the phantom with constant amplitudes and 0° phase difference (b) and 180° phase difference (d).

Results

In Fig. 2, the normalized RF pulse energy, the normalized absorbed energy as well as the ratio between the local and global SAR are presented. The SAR and energies increase about with the square of the reduction factor for lower reduction factors up to six [10]. The ratio of local to global SAR is rather constant and even slightly decreases with increasing reduction factors, which corresponds to previous findings [11,12]. With increasing reduction factors *R*, the distance between the spiral revolutions in k-space increases. Its relation with the desired excitation pattern seems to have a significant impact on the pulse energy, SAR and RMS.

The thermal image of the experimental setup is shown in Fig. 3. The red square indicates the area of the phantom investigated. The spatial distribution of SAR as obtained by simulations (Fig. 4a and c) and as measured by thermal photography (Fig. 4b and d) exhibit a high correlation (Fig.4 a with b and c with d).

Discussion and Conclusion

The resulting SAR strongly depends on the excitation patterns and reduction factors for Transmit SENSE in whole body applications. Furthermore, the SAR strongly depends on additional boundary conditions, e.g., the selected k-space trajectory [13], regularization parameters, and the coil geometries [14]. In analogy with the receive SENSE g-factor describing the noise amplification, the reduction factor describes the SAR increase for Transmit SENSE as proposed by [15].

Further investigations are required on parameters influencing the worst case (local) SAR to guarantee patient safety on multi-transmit MRI systems.

The distribution of the electric field cannot be determined easily using MRI measurements, but the corresponding temperature distribution can be measured. A good correlation was found between the measured temperature and SAR simulations. Therefore, the FDTD method is a valuable tool for (local) SAR estimation to guarantee patient safety on multi-channel transmission MRI systems.

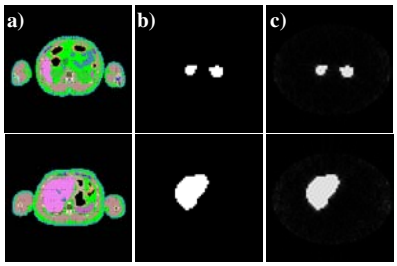

Fig. 1: Selected transversal slices of the bio-mesh color-coding material properties (a). Target- (b) and calculated excitation pattern (Bloch-simulation) (c) of the kidney (top) and liver (bottom).

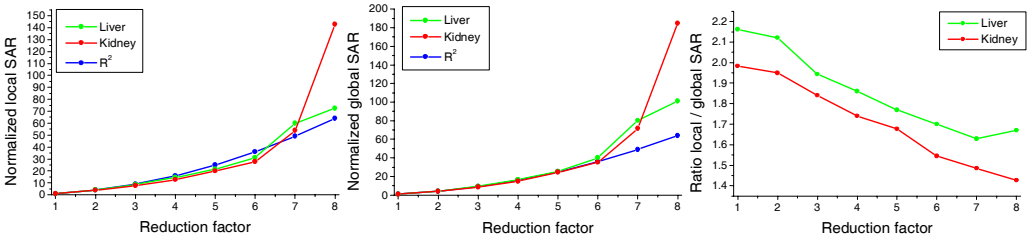

Fig. 2: Simulations results for reduction factor one to eight:
a) Normalized local SAR, b) Normalized global SAR, and c) Ratio of local to global SAR.
A reduction factor of eight represents the maximum pulse acceleration possible with the eight-element array.

References

[1] Katscher U, et al. [2003] MRM 49:144-150	[2] Zhu Y, et al. [2004] MRM 51:775-764	[3] Ullmann P, et al. [2005] MRM 54:994-1001
[4] Junge S, et al. [2004] ISMRM 12:41	[5] Wuebbeler G, et al. [2004] ISMRM 12:665	[6] Vernickel P, et al. [2006] ISMRM 14:123
[7] "Visible Human Project" NLM [1996]	[8] Graesslin I, et al. [2006] ISMRM 14:2470	[9] Graesslin I, et al. [2006] ISMRM 14:129
[10] Katscher U, et al. [2005] ISMRM 13:17	[11] Ullmann P, et al. [2006] ISMRM 14:601	[12] Graesslin I, et al. [2006] MAGMA 19:S18
[13] Conolly S, et al. [1988] JRM 78:440–458	[14] Katscher U, et al. [2005] MAGMA 18(2):81-88	[15] Zhu [2006] ISMRM 14:599